

# Extending the Operating Line Methodology to Consider Shaft and Preheating Injections in Blast Furnaces

Manuel BAILERA,<sup>1,2)\*</sup> Takao NAKAGAKI<sup>1)</sup> and Ryoma KATAOKA<sup>1)</sup>

1) Graduate School of Creative Science and Engineering, Waseda University, Okubo, Shinjuku-ku, Tokyo, 169-8555 Japan.  
 2) Escuela de Ingeniería y Arquitectura. Universidad de Zaragoza, Campus Río Ebro, María de Luna 3, 50018, Zaragoza, Spain.

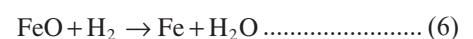
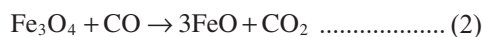
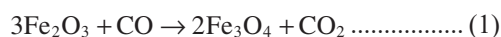
(Received on March 14, 2022; accepted on May 10, 2022; J-STAGE Advance published date: August 18, 2022)

In the last years, the injection of reducing gases in the shaft and preparation zone of the blast furnace has been proposed as a decarbonization option, mainly associated to oxyfuel blast furnaces and top gas recycling configurations. However, the Rist diagram, which is one of the preferred methodologies to characterize the operation of blast furnaces, is not valid to evaluate these new decarbonization options. In this article we propose a generalization of the operating line methodology to extend its applicability to scenarios of variable molar flows along the blast furnace (*i.e.*, shaft and preheating injections) and non-continuous oxidation profiles (presence of CO<sub>2</sub> and H<sub>2</sub>O in the injected gases). The extended operating line methodology was implemented in an Aspen Plus simulation, which provides a detailed modelling of the preparation zone, the thermal reserve zone, the lower zone and the raceways. The simulation was used to validate the generalized operating line methodology through three different data sets: (i) an air-blown blast furnace with pulverized coal injection and O<sub>2</sub> enrichment, (ii) an oxyfuel blast furnace with shaft gas injection, and (iii) an oxyfuel blast furnace with preheating gas injection in the preparation zone. In general, the discrepancy between the reference data and the simulation results is well below 3.5%, so the extended operating line methodology is considered validated.

KEY WORDS: rist diagram; oxygen blast furnace; ironmaking; oxyfuel; CO<sub>2</sub>.

## 1. Introduction

The ironmaking industry is among the most energy- and carbon-intensive industries in the world, producing more than 1 800 Mt of crude steel every year.<sup>1)</sup> It is the second largest consumer of industrial energy (7 200 TWh/y),<sup>2)</sup> and responsible of 9% of the total CO<sub>2</sub> emissions worldwide (3.7 Gt<sub>CO2</sub>/y).<sup>1,3)</sup> The main manufacturing process for the production of iron is based on blast furnace technology.<sup>4,5)</sup> In blast furnaces, iron ore and coke are introduced at the top. The iron oxide is reduced while descending, thanks to a reducing gas that ascends in counter-current. The reducing agents are CO (Eqs. (1) to (3)) and H<sub>2</sub> (Eqs. (4) to (6)).<sup>6)</sup> This gas is produced at the lower part of the furnace by burning the coke with O<sub>2</sub>-enriched air that is injected through the tuyeres. Auxiliary fuels, such as pulverized coal or natural gas can be also injected through the tuyeres to decrease the coke input (Fig. 1).<sup>7)</sup>



Because of requiring high-temperature heat (above 800–1 200°C) and the nature of the process itself (CO<sub>2</sub> release during reduction), the blast furnace ironmaking process cannot be decarbonized with direct electrification.<sup>8)</sup>

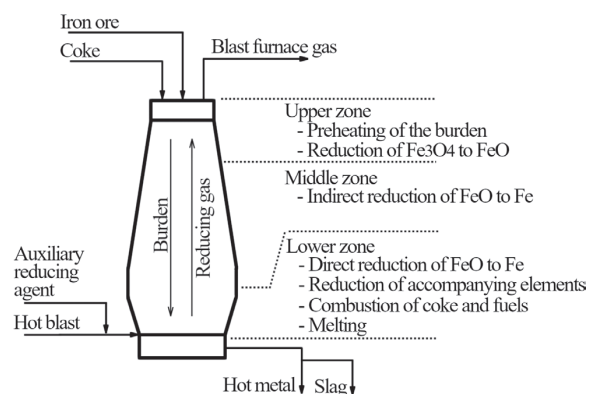


Fig. 1. Conceptual diagram of a blast furnace.

\* Corresponding author: E-mail: mbailera@unizar.es

For this reason, different decarbonization alternatives are proposed and studied in literature, such as the utilization of renewable fuels (CO<sub>2</sub> emissions cuts by 8%–19% can be achieved by using electrolysis power capacities of about 400–900 MW<sup>9–12</sup>), and the injection of reducing gases in the shaft (mid zone)<sup>13–15</sup> and preparation zone (upper zone)<sup>16,17</sup> of the blast furnace (what allows increasing the amount of synthetic fuels that can be inject, since the flame temperature is not affected).

One of the preferred methodologies to evaluate this type of new operating configurations is the Rist diagram (also known as operating diagram, or operating line). The operating line of a blast furnace is the graphical representation of the mass and energy balances concerning the formation of the reducing gas (range 0 < X < 1 in a Cartesian plot) and its utilization to reduce the iron ore (range 1 < X < 2 of the plot). This methodology was firstly proposed by Rist *et al.*,<sup>18</sup> and recently revisited by Bailera *et al.*<sup>19</sup> to account for multiple injections in the tuyeres. However, two restrictive conditions must be assumed: (i) a constant ratio along the blast furnace between the moles of reducing gas and the moles of Fe produced, and (ii) the absence of oxidized gases at the beginning of the indirect reduction process. The first condition is not met when injecting gases in the shaft or preheating zone, while the second is not fulfilled when the synthetic gases have CO<sub>2</sub> or H<sub>2</sub>O contents. For this reason, the conventional operating diagram is not valid when aiming for evaluating new blast furnace decarbonization concepts.

In this study, we extend the operating line methodology by proposing a novel generalized model that is able to deal with gas injections at any part of the blast furnace, including oxidized compounds. This is of special interest when studying new decarbonization concepts. Moreover, to validate the methodology, this is implemented in a detailed Aspen Plus simulation that includes individual models of the preparation zone, the thermal reserve zone, the lower part and the raceways. Other Aspen Plus models found in literature neither were explained with the sufficient level of detailed to be reproducible by other authors, nor present a satisfactory level of detail and separation of the different zones mentioned.<sup>20–23</sup>

The paper is divided in the following sections: first, the extended operating line methodology is introduced (Section 2); then, the calculation method of the extended operating line is explained (Section 3); third, a novel Aspen Plus simulation that implements the proposed extended methodology is presented (Section 4); finally, the model is validated using data from three different types of blast furnaces, including tuyere, shaft and preheating injections (Section 5).

**2. Definition of the Extended Operating Line**

In this study, we extend the operating line methodology to consider gas injections at any part of the blast furnace (*i.e.*, no constant mole flow along the BF), and the possibility of injecting gas that already contains oxidized components (*i.e.*, a non-continuous oxidation profile during the gas ascent). To include these features while keeping the same methodology basis, the definition of the diagram is modified. In the region 0 < X < 1 it must be considered the mole flow of the final blast furnace gas, instead of only the mole flow of CO and H<sub>2</sub> after the raceways, while the region 1 < X < 2 must reflect the transfer of O from the iron ore to the gas, rather than the oxidation state of the gas. This way, we use the ratio between the mole flow of the final blast furnace gas and the moles of Fe produced to combine the two regions in a single Cartesian diagram, since this ratio will remain constant independently of the place, type and number of gas injections.

**2.1. Extended Operating Line in the Range 0 < X < 1: Formation of the Gas**

The region 0 < X < 1 of the operating diagram is the sum

of the number of moles that each injection or reaction provides to the total blast furnace gas, in a unitary basis. Therefore, the units of each addend in the abscissa axis will be those of Eq. (7), where *n<sub>i,j</sub>* is the number of moles of component *i* produced by the reaction or injection *j* (we exclude the N<sub>2</sub> for simplicity, since this is considered an inert inside the furnace).

$$X = \frac{\sum_i n_{i,j}}{\sum_{i,j} n_{i,j}} \dots\dots\dots (7)$$

The total sum will be equal to 1, and it is given by Eq. (8), where *x<sub>v</sub>* denotes the CO produced when the O<sub>2</sub> of the hot blast react with C. The term 2*x<sub>e</sub>* accounts for the H<sub>2</sub> and CO produced by the moisture of the hot blast when dissociated through C. The terms *x<sub>up</sub>* and *x<sub>mid</sub>* are the mole flows of injections in the upper and mid part of the blast furnace. The term *x<sub>mb</sub>* is for the moisture entering with the burden at the top. The term *a<sub>j</sub>x<sub>j</sub>* denotes the H<sub>2</sub> from the incomplete combustion of an auxiliary injection *j* at the tuyeres, while 2*b<sub>j</sub>x<sub>j</sub>* is the CO produced when the oxygen of that auxiliary injection reacts with C. The terms *x<sub>Si</sub>*, *x<sub>Mn</sub>* and *x<sub>P</sub>* stand for the CO produced when reducing the impurities SiO<sub>2</sub>, MnO and P<sub>2</sub>O<sub>5</sub>. The addend *x<sub>S</sub>* represents the CO released when transferring the dissolved Sulphur in the iron to the slag. The term *x<sub>k</sub>* is the H<sub>2</sub> directly coming from the hydrogen content of the coke. Lastly, *x<sub>d</sub>* denotes the moles of gas that were produced during the direct reduction of wüstite. A more detailed description of all these reactions can be found in conventional operating diagram methodologies.<sup>19</sup>

$$x_v + 2x_e - x_e + x_{up} + x_{mid} + x_{mb} + \sum (a_j + 2b_j)x_j - x_{CO2,j} - x_{H2O,j} + x_{Si} + x_{Mn} + x_P + x_S + x_k + x_d = 1 \dots\dots\dots (8)$$

The similar mole balance can be performed per unit of mole of Fe produced in the blast furnace, where the units of each addend in the ordinate axis are given by Eq. (9). The sum of all the addends is denoted by *μ* (Eq. (10)), which corresponds to the slope of the operating line by construction. In other words, *μ* is the number of moles contained in the outlet blast furnace gas per mole of Fe produced (excluding the N<sub>2</sub>), Eq. (11).

$$Y = \frac{\sum_i n_{i,j}}{n_{Fe}} \dots\dots\dots (9)$$

$$y_v + 2y_e - y_e + y_{up} + y_{mid} + y_{mb} + \sum (a_j + 2b_j)y_j - y_{CO2,j} - y_{H2O,j} + y_{Si} + y_{Mn} + y_P + y_S + y_k + y_d = \mu \dots\dots\dots (10)$$

$$\mu = \frac{\sum_{i,j} n_{i,j}}{n_{Fe}} \dots\dots\dots (11)$$

When representing this two proportional sums (*i.e.*, Eqs. (8) and (10)) in a Cartesian plot (**Fig. 2**), the intercept is arbitrary. For convenience, it is chosen so that the moles that have reduced or will reduce one mole of oxygen atom from the iron ore by direct reduction appear in the positive side of the ordinate axis (*i.e.*, *y<sub>d</sub>* in the positive side). Thus, the intercept *Y<sub>E</sub>* is given by Eq. (12).

$$Y_E = -\left(y_v + 2y_e - y_e + y_{up} + y_{mid} + y_{mb} + \sum (a_j + 2b_j)y_j - y_{CO2,j} - y_{H2O,j} + y_{Si} + y_{Mn} + y_P + y_S + y_k\right) \dots\dots\dots (12)$$

It must be noted that the CO<sub>2</sub> and H<sub>2</sub>O entering at the tuyeres will be reduced by C producing two moles of reducing gas (Eq. (13) or Eq. (14)), later followed by the indirect reduction process (Eq. (3) or Eq. (6)). The overall reaction is actually the direct reduction process (Eq. (15) or Eq. (16)),

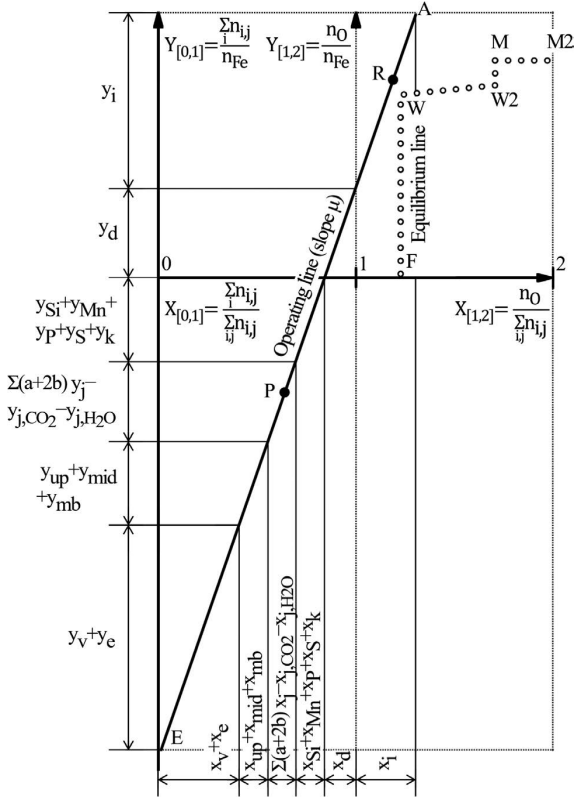
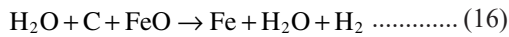
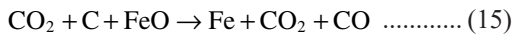
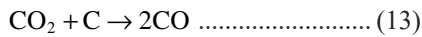


Fig. 2. Extended operating line.

where one of the two generated moles of gas has gained one mole of oxygen atom transferred from the iron oxides.



Therefore, to properly quantify the direct reduction in the operating line, half of the moles produced because of the injection of CO<sub>2</sub> and H<sub>2</sub>O at the tuyeres must be accounted in the addend y<sub>d</sub>. For this reason, the terms x<sub>e</sub>, x<sub>CO<sub>2,j</sub></sub> and x<sub>H<sub>2</sub>O,j</sub> are subtracted in Eq. (8). Otherwise, the percentage of direct reduction would be underestimated, as occurs in conventional operating diagrams, which wrongly predicts decreases in the direct reduction when injecting CO<sub>2</sub> and H<sub>2</sub>O.

**2.2. Extended Operating Line in the Range 1 < X < 2: Oxygen Transferred to the Gas**

The region 1 < X < 2 of the operating diagram quantifies the atoms of O transferred from the iron oxides to the blast furnace gas by indirect reduction. In order to plot this value in the same Cartesian diagram, we need to use the same proportionality than in the range 0 < X < 1. Therefore, the abscissas will use the units of Eq. (17), and the ordinates the units of Eq. (18).

$$X = \frac{n_o}{\sum_{i,j} n_{i,j}} \dots\dots\dots (17)$$

$$Y = \frac{n_o}{n_{Fe}} \dots\dots\dots (18)$$

Contrarily to the conventional methodology, the range 1 < X < 2 in the newly proposed diagram does not reflect the oxidation state of the gas. In this case, it represents the number of O atoms transferred to the gas, per total number of

moles in the final blast furnace gas (abscissas) or per moles of Fe produced in the blast furnace (ordinates).

It should be noted that the whole range 0 < X < 2, in the positive side of the ordinates, quantifies the total O reduced from the iron oxides (by both, direct and indirect reduction), thanks to our proper definition of the term y<sub>d</sub> and the convenient intercept of the operating line. Thus, the point Y<sub>A</sub> in the operating line is still the initial oxidation state of the burden, as in conventional methodologies.

**3. Calculation of the Extended Operating Line and Information Resulting Therefrom**

As in conventional methodologies, the extended operating line is obtained by the calculation of two characteristic points (P and R) to compute the slope (Eq. (19)) and the intercept (Eq. (20)).

$$\mu = \frac{Y_R - Y_P}{X_R - X_P} \dots\dots\dots (19)$$

$$Y_E = Y_R - X_R \left( \frac{Y_R - Y_P}{X_R - X_P} \right) \dots\dots\dots (20)$$

The point P is related to the energy balance of the blast furnace, and the point R to the approach to chemical equilibrium that exists in the thermal reserve zone. The former can be easily extended to the scenario of injections in the middle and upper part just by adding additional terms in the energy balance, while the latter requires changing the frame of reference of the Chaudron diagrams.

**3.1. Point P: Energy Balance**

The energy balance in the elaboration zone, Eq. (21), makes the operating line to pass through a point of coordinates X<sub>P</sub> and Y<sub>P</sub> (Eqs. (22) and (23)), where A, B, C and Y<sub>E</sub><sup>\*</sup> are given by Eqs. (24) to (27).

$$q_c y_v + q_v y_v + (q_{iw} Y_w - \delta) = q_g (y_d - y_e - y_{CO_2,j} - y_{H_2O,j}) + q_k y_k + q_e y_e + \sum q_j y_j - \delta' + q_{Si} y_{Si} + q_{Mn} y_{Mn} + q_P y_P + q_\gamma \gamma + f + l + p + C_{\Delta T_R} + q_{mid} y_{mid} \dots\dots\dots (21)$$

$$X_P = \frac{B(1+2e)}{A+B(1+2e)} \dots\dots\dots (22)$$

$$Y_P = Y_E^* - \left( \frac{C}{B} + Y_E^* \right) \left( \frac{B(1+2e)}{A+B(1+2e)} \right) \dots\dots\dots (23)$$

$$A = q_c + q_v - eq_e + eq_k (1-r) + eq_g \dots\dots\dots (24)$$

$$B = q_g \dots\dots\dots (25)$$

$$C = -q_{iw} Y_w + \delta + q_k y_k + \sum q_j y_j - (1-r)(y_k + \sum a_j y_j) q_k + q_{Si} y_{Si} + q_{Mn} y_{Mn} + q_P y_P + q_\gamma \gamma + f + l + p + C_{\Delta T_R} - q_g (y_{CO_2,j} + y_{H_2O,j}) + q_{mid} y_{mid} \dots\dots\dots (26)$$

$$Y_E^* = -(y_{up} + y_{mid} + y_{mb} + \sum (a_j + 2b_j) y_j - y_{CO_2,j} - y_{H_2O,j} + y_{Si} + y_{Mn} + y_P + y_S + y_k) \dots\dots\dots (27)$$

The mathematical derivation of these coordinates, as well as the calculation of the individual terms of the energy balance, follows the same procedure as for the conventional operating diagram (see the work of Bailera *et al.*<sup>19,24</sup>) for more details). The only new terms in the energy balance

are those related to the injection of CO<sub>2</sub> and H<sub>2</sub>O through the tuyeres, and to the sensible heat of the gas injected in the middle zone. The former diminishes the heat consumed by the tuyere injections by  $q_g(y_{CO_2,j} + y_{H_2O,j})$  because this amount will be already taken into account in the term  $q_g y_d$ . The latter adds a heat consumption equal to  $q_{mid} y_{mid}$ , which is used to heat the shaft injection up to the reference temperature (thermal reserve zone temperature). The injection of gas in the upper zone and the presence of moisture in the burden do not affect the energy balance because the control volume is restricted to the mid and lower zone.

**3.2. Point R: Thermal Reserve Zone**

The point R is calculated as a function of the approach to the equilibrium of the Fe–O–H–C system in the thermal reserve zone. This approach is quantified by the chemical efficiency, which is the ratio between the O atoms actually exchanged and the O atoms that would be exchanged at equilibrium. Since the initial oxidation state of the burden is  $Y_A$ , and the oxidation at chemical equilibrium in the thermal reserve zone corresponds to pure wüstite (*i.e.*,  $Y_W = 1.05$ ), the ordinates of the point R are given by Eq. (28).

$$Y_R = Y_A - r(Y_A - Y_W) \dots\dots\dots (28)$$

The abscissas of the point R are calculated from the oxidation state of the gas that is in equilibrium with pure wüstite,  $\omega_{OHC}$  (Eq. (29)). This value combines the individual Chaudron diagrams of the Fe–O–C and Fe–O–H systems (Eqs. (30) and (31))<sup>19)</sup> by using the ratio of H<sub>2</sub> moles in the gas,  $x_h$  (Eq. (32)). The latter must be calculated at the thermal reserve zone (*i.e.*, without accounting for the injections in the upper zone or the moisture of the burden).

$$\omega_{OHC} = (1 - x_h)\omega_{OC} + x_h\omega_{OH} \dots\dots\dots (29)$$

$$\omega_{OC} = 0.4089 + 3.8856 \cdot 10^{-3} T_R - 1.3778 \cdot 10^{-5} T_R^2 + 1.7924 \cdot 10^{-8} T_R^3 - 1.0465 \cdot 10^{-11} T_R^4 + 2.3054 \cdot 10^{-15} T_R^5 \dots (30)$$

$$\omega_{OH} = -0.0496 - 0.5075 \cdot 10^{-3} T_R + 0.4367 \cdot 10^{-5} T_R^2 - 0.6745 \cdot 10^{-8} T_R^3 + 0.4402 \cdot 10^{-11} T_R^4 - 1.0668 \cdot 10^{-15} T_R^5 \dots (31)$$

$$x_h = \frac{n_{H_2} + n_{H_2O}}{n_{CO} + n_{CO_2} + n_{H_2} + n_{H_2O}} \dots\dots\dots (32)$$

In order to plot this oxidation state of the gas in the extended diagram, the value must be converted taking into account the chemical efficiency, the total mole flow of the BFG, and the chemical species that were already oxidized before the indirect reduction stage. In other words, we calculate the moles of O atoms that were transferred to this gas by indirect reduction, per mole of blast furnace gas (Eq. (33)).

$$X_R = \frac{r\omega_{OHC}(\mu - y_{up} - y_{mb}) - (y_{CO_2,mid} + y_{H_2O,mid} + y_{CO_2,j} + y_{H_2O,j} + y_e)}{\mu} \dots\dots\dots (33)$$

The factor  $(\mu - y_{up} - y_{mb})/\mu$  changes the frame of reference to consider the whole gas, instead of only the gas in the chemical reserve zone, while the factor  $(y_{CO_2,mid} + y_{H_2O,mid} + y_{CO_2,j} + y_{H_2O,j} + y_e)/\mu$  subtracts the chemical species that were already oxidized before the transfer of O by indirect reduction. By substituting Eq. (19) in Eq. (33), we find Eq. (34), where D, E, F are given by Eqs. (35) to (37).

$$X_R = \frac{D(Y_R - Y_P) + (E + F)X_P}{Y_R - Y_P + E + F} \dots\dots\dots (34)$$

$$D = r\omega_{OHC} + 1 \dots\dots\dots (35)$$

$$E = r\omega_{OHC}(y_{up} + y_{mb}) \dots\dots\dots (36)$$

$$F = (y_{CO_2,mid} + y_{H_2O,mid} + y_{CO_2,j} + y_{H_2O,j} + y_e) \dots (37)$$

It can be seen that, if there are no injections in the mid and upper zone, and there are neither injection of CO<sub>2</sub> and H<sub>2</sub>O in the tuyeres, the value of  $X_R$  in Eq. (34) is the same as for the conventional operating line methodology.

**3.3. Additional Results Derived from the Operating Line**

Characterizing the extended operating line allows deriving the coke consumption (Eq. (38)), the air flow rate (Eq. (39)), the oxidation state of the blast furnace gas (*i.e.*, the gas utilization, Eq. (40)), and the percentage of direct reduction (Eq. (41)).

$$m_K = \frac{\mu + \frac{10^6 \Omega_{HM,C}}{M_C n_{Fe}} - e y_v - \sum(\tau_j + a_j) y_j - y_{up} - y_{mid} - y_{mb}}{10^3 \left( \frac{\Omega_{K,C}}{M_C} + \frac{\Omega_{K,H}}{M_{H_2}} \right)} \dots\dots\dots (38)$$

$$m_{air} = \frac{y_v n_{Fe} \left( M_{O_2} + \frac{0.79}{0.21} M_{N_2} \right)}{2000(1 - \Omega_{air,H_2O})} \dots\dots\dots (39)$$

$$\eta_{CO,H_2} = \frac{Y_A - Y_E + F + y_{CO_2,up} + y_{H_2O,up} + y_{mb}}{\mu} - 1 \dots (40)$$

$$y_{d,\%} = \frac{\mu + Y_E}{Y_A} \cdot 100 \dots\dots\dots (41)$$

The derivation of these equations is similar to the conventional methodology,<sup>19)</sup> but adapted to the frame of reference of the extended operating line. The meaning and units of the different variables is specified in the nomenclature section.

**4. Simulation in Aspen Plus**

The extended operating line was implemented in Aspen Plus to validate the novel proposed methodology. The modelled blast furnace was divided in upper, mid and lower zone, with the latter including the raceways (Fig. 3). Considering the whole blast furnace as the boundary, there are 10 inlet mass streams, three outlet mass streams and one outlet heat stream. The model calculates the mass flow of coke, air, hot metal, slag and BFG, and the composition of the two latter, as a function of the temperature of the thermal reserve zone, the chemical efficiency, the heat removed by the staves in the preparation and in the elaboration zone, and the data specified as Input in Table 1. All blocks shown in Fig. 3 are summarized in Table 2, and the complete list of manipulators is presented in Table 3.

The upper zone consists of a stoichiometric reactor where the hematite is reduced to magnetite and wüstite. The inlets are the iron ore, the coke, the gas ascending from the thermal reserve zone, and (if present) a gas injection for preheating. The outlets are the blast furnace gas, and the solids descending to the mid zone. The extent of the iron ore reduction depends on the chemical efficiency, which sets the oxidation state of the burden descending to the mid zone (*i.e.*, to the thermal reserve zone). Moreover, the fraction of this reduction that takes place via H<sub>2</sub> is set according to the energy balance in the preparation zone. Two modelling options are considered for the energy balance: i) fixing the outlet temperature of the BFG, letting free the H<sub>2</sub> utilization (UPA design spec), or ii) fixing the H<sub>2</sub> utilization, letting free the outlet temperature of the BFG (UPB design spec). It should be noted that the reduction by H<sub>2</sub> is considered as the combination of the reduction by CO plus the reverse

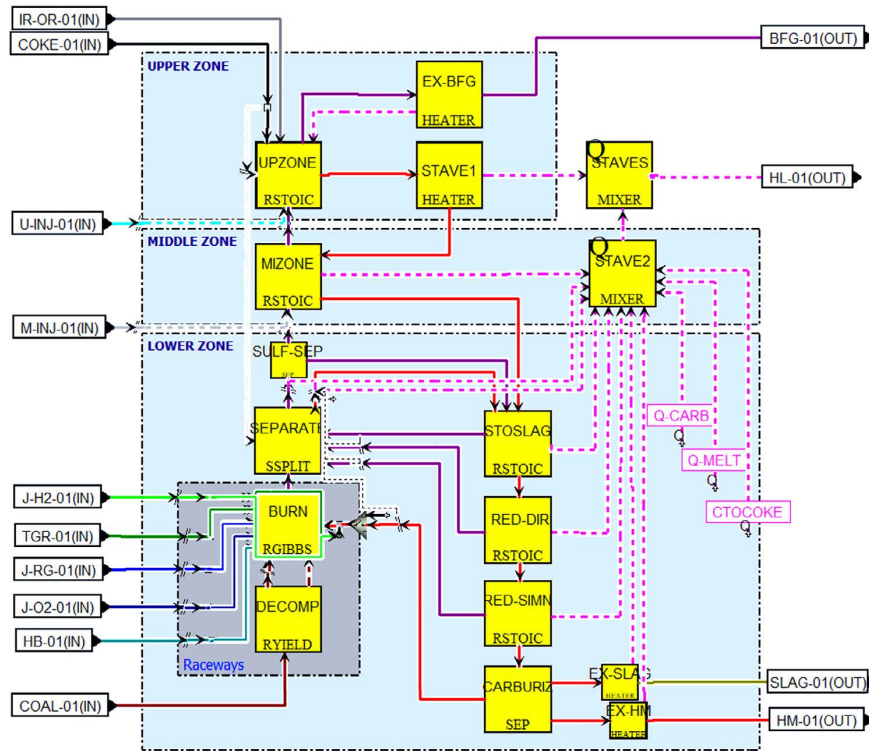


Fig. 3. Process flow diagram of a blast furnace in Aspen Plus. (Online version in color.)

**Table 1.** Summary of model input/output data regarding the streams crossing the boundary of the blast furnace.

Stream	Description	Flow	Composition	Temperature
IR-OR-01	Iron ore	Input	Input	Input
COKE-01	Coke	Output	Input	Input
HB-01	Air + moisture	Output	Input	Input
COAL-01	Pulverized coal injection at tuyeres	Input	Input	Input
J-O2-01	O <sub>2</sub> injection for enrichment at tuyeres	Input	Input	Input
J-H2-01	H <sub>2</sub> injection at tuyeres	Input	Input	Input
J-RG-01	Gas injection at tuyeres	Input	Input	Input
TGR-01	Top gas recirculation injected at tuyeres	Input	Input	Input
M-INJ-01	Gas injection at mid shaft	Input	Input	Input
U-INJ-01	Gas injection at upper part	Input	Input	Input
HM-01	Hot metal	Output	Input	Input
SLAG-01	Slag	Output	Output	Input
BFG-01	Blast furnace gas	Output	Output	Input/Output
HL-01	Heat removed by the staves	Input/Output	–	–

water-gas shift reaction.

The mid zone uses a stoichiometric reaction to consider the indirect reduction of magnetite to wüstite, and of the wüstite to iron. The inlets are the solids descending from the upper part, the gas ascending from the lower part, and (if exists) a reducing gas injection (shaft injection). The outlets are the gas ascending to the upper zone, and the solids descending to the lower zone. The extent of the reduction is set according to the percentage of indirect reduction cal-

culated by the extended operating line methodology. The fraction of this reduction taking place via H<sub>2</sub> is set according to the chemical efficiency and the Chaudron diagram of the Fe–O–H system at the temperature of the thermal reserve zone. It should be noted that, since the H<sub>2</sub> participation is not set according to the energy balance, the net heat removed by the staves in the elaboration zone will be an output of the simulation. Nevertheless, since it is used as an input in the calculation of the extended operating line, both values must be the same (discrepancy is below 0.5%).

The lower zone gathers five processes: the complete transfer of sulphur to the slag, the direct reduction of the remaining wüstite, the reduction of the accompanying elements (whose extent is given as a function of the desired hot metal composition), the carburization process (set according to the C content in hot metal), and the melting of slag and hot metal. The heats of carburization and melting are calculated separately, since Aspen Plus cannot deal with this type of thermodynamic processes. The inlets to these processes are the solids descending from the mid zone, and the ashes and sulfur from the combustion of coal in the raceways. The outlets are the CO produced in these processes (which will be mixed with the raceways gas and sent to the mid zone), the remaining carbon after carburization (which is sent to the raceways at 1 200°C for combustion), and the final hot metal and slag.

The raceways consist of the decomposition of the coal through a Yield reactor (considered as a non-conventional solid in Aspen Plus), and the calculation of the chemical equilibrium of the combustion by a Gibbs reactor. The inlets are the injections of the auxiliary reducing agents, the air, and the coke carbon not consumed in other processes. The outlet is the raceway gas (whose temperature corresponds to the adiabatic flame temperature), and the sulphur and ashes (diverted to the processes of the lower zone). The raceway gas is mixed with the CO produced in the lower zone, and then sent to the mid zone.

The model was developed in Aspen Plus v11, using the PENG-ROB property method<sup>25)</sup> for the gas streams. In the case of non-conventional solids (*i.e.*, coal), it was used the HCOALGEN and DCOALIGT property models with the following correlations:<sup>26)</sup> (i) Revised IGT correlation for the

**Table 2.** Main blocks of the Aspen Plus simulation.

Block	Type	Process and reactions	Manipulator
UPZONE	Stoichiometric reactor	$3\text{Fe}_2\text{O}_3 + \text{CO} \rightarrow 2\text{Fe}_3\text{O}_4 + \text{CO}_2$	CHEM-EFF
		$\text{Fe}_3\text{O}_4 + \text{CO} \rightarrow 3\text{FeO} + \text{CO}_2$	UPA
		$\text{CO}_2 + \text{H}_2 \rightarrow \text{CO} + \text{H}_2\text{O}$	
EX-BFG	Heater	It sets the outlet temperature of the blast furnace gas, and returns the excess heat to the upper zone.	UPB
STAVE1	Heater	It sets the temperature at TRZ for the solids descending to the mid zone, and provides the excess heat to the staves.	–
MIZONE	Stoichiometric reactor	$\text{Fe}_3\text{O}_4 + \text{CO} \rightarrow 3\text{FeO} + \text{CO}_2$	YDR
		$\text{FeO} + \text{CO} \rightarrow \text{Fe} + \text{CO}_2$	XR
		$\text{CO}_2 + \text{H}_2 \rightarrow \text{CO} + \text{H}_2\text{O}$	
STAVE2	Q-Mixer	It gathers all the heat streams of the mid and lower zone and provides the net value to the staves.	–
STAVES	Q-Mixer	It gathers the net heat streams of the upper, mid and lower zone. The output is the total heat removed by the staves.	–
SULF-SEP	Separator	It diverts the Sulphur to the block STOSLAG.	–
SEPARATE	Splitter	It gathers all the gases produced in the lower part and the ashes from coal combustion. It separates the gases (sent upwards to the mid zone) and the solids (sent downwards).	–
BURN	Gibbs reactor	It calculates the chemical equilibrium for combustion and the flame temperature.	–
DECOMP	Yield reactor	It decomposes the coal (non-conventional solid) into C, H <sub>2</sub> , O <sub>2</sub> , N <sub>2</sub> , S, SiO <sub>2</sub> , Al <sub>2</sub> O <sub>3</sub> and CaO to perform calculations.	COMBUST
STOSLAG	Stoichiometric reactor	$\text{Fe} + \text{S} \rightarrow \text{FeS}$	–
		$\text{FeS} + \text{CaO} + \text{C} \rightarrow \text{Fe} + \text{CaS} + \text{CO}$	
RED-DIR	Stoichiometric reactor	$\text{FeO} + \text{C} \rightarrow \text{Fe} + \text{CO}$	–
RED-SIMN	Stoichiometric reactor	$\text{SiO}_2 + 2\text{C} + 3\text{Fe} \rightarrow \text{Fe}_3\text{Si} + 2\text{CO}$	HM-SI
		$\text{MnO} + \text{C} \rightarrow \text{Mn} + \text{CO}$	HM-MN
CARBURIZ	Separator	It separates solids into slag (SiO <sub>2</sub> , Al <sub>2</sub> O <sub>3</sub> , CaO, MgO, MnO, CaS) and hot metal (Fe, C, Fe <sub>3</sub> Si, Mn). The remaining C is sent to the burner.	HM-C
EX-SLAG	Heater	It sets the outlet temperature of the slag.	–
EX-HM	Heater	It sets the outlet temperature of the hot metal.	–

**Table 3.** Manipulators of the Aspen Plus simulation.

Manipulator	Type	Description	Modifies
CHEM-EFF	Design spec	It modifies the extent of Fe <sub>3</sub> O <sub>4</sub> reduction according to the chemical efficiency, in order to set the oxidation state of the burden descending to the mid zone equal to Y <sub>R</sub> (extended operating diagram).	UPZONE
UPA	Design spec	It modifies the extent of reverse water-gas shift reaction according to the heat removed by the staves in the upper zone. The temperature of the BFG is assumed to be known (when UPA is used, UPB is deactivated).	UPZONE
UPB	Design spec	It modifies the outlet temperature of the BFG according to the heat removed by the staves in the upper zone. The H <sub>2</sub> utilization is assumed to be known (when UPB is used, UPA is deactivated).	EX-BFG
YDR	Design spec	It modifies the extent of FeO reduction in the mid zone according to the percentage of indirect reduction calculated by the RIST block.	MIZONE
XR	Design spec	It modifies the extent of reverse water-gas shift reaction in the mid zone according to the chemical efficiency and the equilibrium of the Fe–O–H system at T <sub>R</sub> .	MIZONE
COMBUST	Calculator	It calculates the mass flow of C, H <sub>2</sub> , O <sub>2</sub> , N <sub>2</sub> , S, SiO <sub>2</sub> , Al <sub>2</sub> O <sub>3</sub> and CaO obtained after the decomposition of the coal, as a function of the ultimate analysis, the moisture and the ash composition.	DECOMP
HM-SI	Design spec	It modifies the extent of SiO <sub>2</sub> reduction according to the composition of the hot metal.	RED-SIMN
HM-MN	Design spec	It modifies the extent of MnO reduction according to the composition of the hot metal.	RED-SIMN
HM-C	Design spec	It modifies the C diverted to HM-01 stream according to the composition of the hot metal.	CARBURIZ
QMELT	Design spec	It sets the heat used for melting the hot metal and slag according to their mass flow and composition.	Q-MELT
QCARB	Design spec	It sets the heat used for carburization according to the C content in the hot metal.	Q-CARB
QTOCOKE	Design spec	It sets the heat required to consider C as coke instead as graphite in the energy balances, as a function of the mass flow of coke entering the blast furnace. Aspen provides C as graphite by default.	CTOCOKE
RIST	Calculator	It calculates the mass flow of coke and hot blast (air + moisture) according to the extended operating line methodology.	COKE-01, HB-01

heat of combustion,<sup>27)</sup> (ii) Direct correlation for the heat of formation, (iii) Kirov correlation for the heat capacity, and (iv) IGT correlations for density on a dry basis. In addition, user-defined heat capacities from NIST data base were

used for different chemical components (instead of the data provided by the Aspen Plus data base) to increase the valid range of application up to 2 700 K. The error of the results of the extended operating line methodology (calculated in

a Fortran subroutine in the RIST block) with respect to the results finally obtained in the simulation (adjusted by the different manipulators of Table 3) is <0.1% for the percentage of direct reduction, <0.01% for the percentage of gas utilization, <0.001% for mass balances, and <0.5% for energy balances. The computer used for the simulation runs on 64-bit Windows 10 under a 11th Gen Intel® Core™ i7-1185G7 processor at 3.00 GHz, and 16 GB RAM.

5. Results and Discussion

5.1. Model Validation

The developed simulation has been used to reproduce

the results from three different authors, covering tuyere injections (at the lower zone),<sup>28)</sup> shaft injections (at the mid zone)<sup>14)</sup> and preheating injections (at the upper zone).<sup>16)</sup> The conceptual schemes of these three blast furnaces are shown in Fig. 4, together with a summary of most relevant results. The full streams' composition and BF's operating conditions are gathered in Table 4. Typical mass fractions for the coke, iron oxides and hot metal are assumed according to literature,<sup>21,29)</sup> since the original references do not provide this information.

The first validation is made for an air-blown blast furnace with pulverized coal injection and O<sub>2</sub> enrichment. The reference data was elaborated by Babich *et al.*<sup>28)</sup> (typical values

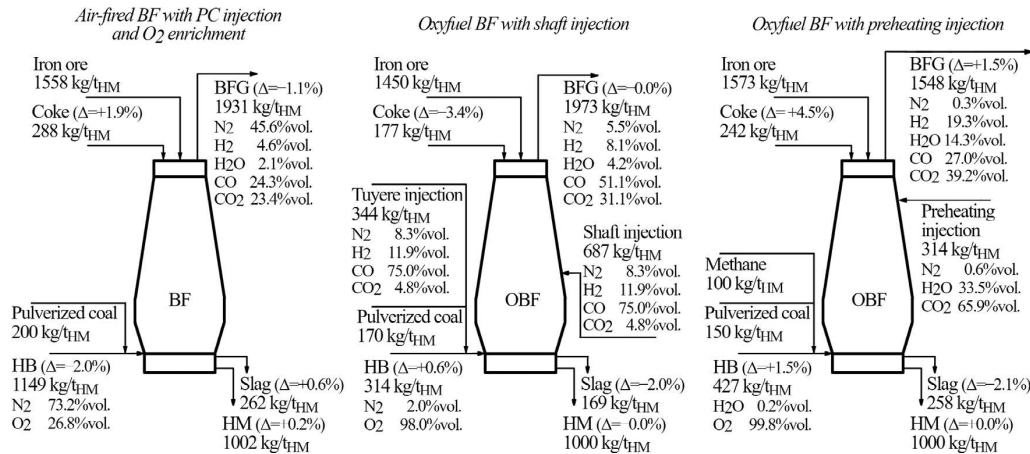


Fig. 4. Conceptual schemes for an air-blown BF with PC injection,<sup>28)</sup> an oxyfuel BF with shaft injection,<sup>14)</sup> and an oxyfuel BF with preheat injection,<sup>16)</sup> summarizing the mass flows, gas compositions, and relative error obtained during the validation of the extended operating line methodology.

Table 4. Validation of the extended operating diagram implemented in Aspen Plus.

	BF with PC injection			OBF with Shaft injection			OBF with Preheat injection		
	Babich <sup>28)</sup>	Model	Δ (%)	Jin <sup>14)</sup>	Model	Δ (%)	Sato <sup>16)</sup>	Model	Δ (%)
Inlet (kg/tHM)									
Iron ore	1 558.0	1 558.0	-	1 450.0	1 450.0	-	1 573.0	1 573	-
# Fe <sub>2</sub> O <sub>3</sub>	-	1 146.9	-	-	820.9	-	-	1 135.0	-
# FeO	-	187.3	-	-	478.8	-	-	196.1	-
# SiO <sub>2</sub>	-	69.9	-	-	36.1	-	-	99.5	-
# Al <sub>2</sub> O <sub>3</sub>	-	107.2	-	-	70.8	-	-	95.2	-
# CaO	-	26.9	-	-	25.0	-	-	27.1	-
# MgO	-	16.2	-	-	15.0	-	-	16.3	-
# MnO	-	3.6	-	-	3.4	-	-	3.7	-
T (°C)	25	25	-	25	25	-	25	25	-
Coke	283.0	288.3	1.9	183.0	176.7	-3.4	232.0	242.4	4.5
# C	-	256.1	-	-	160.5	-	-	226.3	-
# Fe <sub>2</sub> O <sub>3</sub>	-	1.7	-	-	1.1	-	-	1.5	-
# SiO <sub>2</sub>	-	20.0	-	-	8.7	-	-	8.3	-
# Al <sub>2</sub> O <sub>3</sub>	-	9.3	-	-	5.7	-	-	5.4	-
# CaO	-	0.8	-	-	0.5	-	-	0.7	-
# MgO	-	0.3	-	-	0.2	-	-	0.3	-
T (°C)	25	25	-	25	25	-	25	25	-
Coal	200.0	200.0	-	170.0	170.0	-	150.0	150.0	-
# C	153.6	153.6	-	-	139.1	-	-	115.2	-
# H	8.3	8.3	-	-	6.2	-	-	6.2	-
# O	10.2	10.2	-	-	3.6	-	-	7.6	-
# N	3.1	3.1	-	-	1.0	-	-	2.4	-
# S	0.9	0.9	-	-	0.7	-	-	0.6	-
# H <sub>2</sub> O	2.4	2.4	-	-	1.7	-	-	1.8	-
# SiO <sub>2</sub>	12.3	12.3	-	-	10.1	-	-	9.2	-

# Al <sub>2</sub> O <sub>3</sub>	8.9	8.9	–	–	7.3	–	–	6.7	–
# CaO	0.3	0.3	–	–	0.2	–	–	0.2	–
T (°C)	25	25	–	25	25	–	25	25	–
Hot blast	1 172.1	1 148.6	–2.0	312.1	313.9	0.6	420.6	427.0	1.5
# N <sub>2</sub>	826.7	810.1	–2.0	5.5	5.5	0.6	–	–	–
# O <sub>2</sub>	345.4	338.5	–2.0	306.6	308.4	0.6	420.0	426.4	1.5
# H <sub>2</sub> O	–	–	–	–	–	–	0.6	0.6	0.0
T (°C)	1 200	1 200	–	25	25	–	25	25	–
Tuyere injection	–	–	–	343.7	343.7	–	100.0	100.0	–
# N <sub>2</sub>	–	–	–	31.1	31.1	–	–	–	–
# CO <sub>2</sub>	–	–	–	28.3	28.3	–	–	–	–
# CO	–	–	–	281.1	281.1	–	–	–	–
# H <sub>2</sub>	–	–	–	3.2	3.2	–	–	–	–
# CH <sub>4</sub>	–	–	–	–	–	–	100.0	100.0	–
T (°C)	–	–	–	900	900	–	25	25	–
Shaft injection	–	–	–	687.5	687.5	–	–	–	–
# N <sub>2</sub>	–	–	–	62.3	62.3	–	–	–	–
# CO <sub>2</sub>	–	–	–	56.6	56.6	–	–	–	–
# CO	–	–	–	562.2	562.2	–	–	–	–
# H <sub>2</sub>	–	–	–	6.4	6.4	–	–	–	–
T (°C)	–	–	–	900	900	–	–	–	–
Preheat injection	–	–	–	–	–	–	314.2	314.2	–
# N <sub>2</sub>	–	–	–	–	–	–	1.5	1.5	–
# CO <sub>2</sub>	–	–	–	–	–	–	258.9	258.9	–
# H <sub>2</sub> O	–	–	–	–	–	–	53.8	53.8	–
T (°C)	–	–	–	–	–	–	1 000	1 000	–
Outlet (kg/t <sub>HM</sub> )									
Hot metal	1 000.0	1 001.9	0.2	1 000.0	999.9	0.0	1 000.0	1 000.2	0.0
# Fe	–	949.0	–	–	947.4	–	–	947.4	–
# C	–	45.1	–	–	45.0	–	–	45.0	–
# Si	–	5.3	–	–	5.3	–	–	5.3	–
# Mn	–	2.5	–	–	2.5	–	–	2.5	–
T (°C)	–	1 500	–	–	1 500	–	–	1 500	–
Slag	260.0	261.6	0.6	172.3	168.9	–2.0	264.0	258.4	–2.1
# SiO <sub>2</sub>	–	90.8	–	–	43.5	–	–	105.7	–
# Al <sub>2</sub> O <sub>3</sub>	–	125.4	–	–	83.8	–	–	107.3	–
# CaO	–	26.5	–	–	24.5	–	–	26.9	–
# MgO	–	16.5	–	–	15.2	–	–	16.6	–
# MnO	–	0.4	–	–	0.2	–	–	0.5	–
# CaS	–	1.9	–	–	1.6	–	–	1.4	–
T (°C)	1 550	1 550	–	–	1 550	–	–	1 550	–
BFG	1 953.2	1 931.4	–1.1	1 974.0	1 973.4	–0.0	1 525.8	1 548.3	1.5
# N <sub>2</sub>	830.0	813.2	–2.0	100.9	100.1	–0.8	–	4.1	–
# CO <sub>2</sub>	678.8	655.3	–3.5	909.2	886.4	–2.5	–	958.7	–
# CO	414.7	433.3	4.5	904.9	926.9	2.4	–	420.5	–
# H <sub>2</sub> O	23.9	23.7	–0.8	48.7	49.4	1.4	–	143.3	–
# H <sub>2</sub>	5.9	5.9	0.0	10.3	10.5	1.9	21.2	21.6	1.9
T (°C)	150	154	2.7	–	280	–	196	196	–
Parameters									
Chemical efficiency (–)	–	0.92	–	–	1.00	–	0.98	0.98	–
TRZ temperature (°C)	–	850	–	950	950	–	950	950	–
Heat loss (MJ/t <sub>HM</sub> )	701.1	703.7	0.4	–	1 000	–	250.0	250.6	0.2
Flame temperature (°C)	2 117	2 405	13.6	2 227	2 326	4.4	2 267	2 197	–3.1
Gas utilization (%)	48.6	46.8	–3.7	38.4	37.4	–2.6	–	53.6	–

for  $r$  and  $T_R$  were assumed<sup>9,19)</sup>). The simulation results show an error below 3.5% in most cases, what proves that the extended operating line methodology is also valid in the case that no shaft and preheating injections are present. The difference observed in the flame temperature is justified on the control volume of the energy balance of the

raceways. Babich probably included the gas coming from the sub-processes of the lower zone when computing the flame temperature (*i.e.*, the CO coming from the blocks STOSLAG, RED-DIR and RED-SIMN). In our simulation, the temperature of the total ascending gas after mixing is 2 145°C, what gives only a 1.3% error with respect to the



temperature provided by Babich.

The second validation is made for an oxyfuel blast furnace with shaft injection. The reference data of this BF was elaborated by Jin *et al.*<sup>14)</sup> The shaft injection is actually blast furnace gas that has been recirculated after condensing the water and capturing the 90% of the CO<sub>2</sub>. Some of this gas is also injected through the tuyeres as a fuel. The simulation results show a discrepancy below 2.5% in most cases, what validates the extended operating line methodology for blast furnaces with shaft injections.

The third validation is made for an oxyfuel blast furnace with preheating injection (introduced above the thermal reserve zone). The reference data of this blast furnace was elaborated by Sato *et al.*<sup>16)</sup> The preheat injection is actually blast furnace gas that has been burnt with pure O<sub>2</sub>. In this case, no operating parameters had to be assumed, as they were provided by Sato *et al.* The simulation results show a discrepancy below the 3.1% in most cases, so the extended methodology is considered validated also for preheating injections.

The extended operating lines for the three blast furnaces are plotted in Fig. 5. The extended methodology maintains the simplicity of the conventional methodology (*e.g.* in identifying the percentage of direct reduction), while allowing to work with variable molar flows and non-continuous oxidation profiles along the blast furnace. This is particularly noticed when including the phase diagrams in the plot of the operating line. The oxidation state of the gas not necessarily coincides with the range  $1 < X < 2$  of the extended operating diagram, which now stands for the oxygen transferred to the

gas. Thus, for example in the data set of Jin (shaft injection), the gas is already oxidized by 2.1% at the beginning of the mid zone since the gas injected contains CO<sub>2</sub>. Moreover, in the data set of Sato (preheat injection), the oxidation state of the gas changes at the end of the mid zone from 31.8% to 42.7%, because high contents of CO<sub>2</sub> and H<sub>2</sub>O are injected at the upper zone. Therefore, the conditions of the phase diagram also change (in this particular case, the value of  $x_h$  remains the same because the injected gas is actually BFG after its combustion). This axis transformation shows the versatility of the new extended operating diagram, which properly accounts for oxidized gases and injections at the mid and upper zone. Trying to construct the operating line under these conditions by using the original Rist diagram would lead to incorrect results.

## 5.2. Comparing the Results of the Original Rist Model and the New Extended Operating Diagram

In order to proof that the conventional operating diagram is not valid when evaluating OBF with mid and upper injections, we compare the results obtained by both methodologies. In the case of the original Rist diagram,<sup>19)</sup> all injections must be considered within the term  $\sum (a_j + 2b_j)x_j$  of Eq. (8), regardless of their oxidation state and the location of the injection. The results directly computed from the operating lines are shown in Table 5.

In the first case (air-blown BF with pulverized coal injection), both models provide the same results. This is because (i) the ratio along the blast furnace between the moles of reducing gas and the moles of Fe produced is constant (*i.e.*,

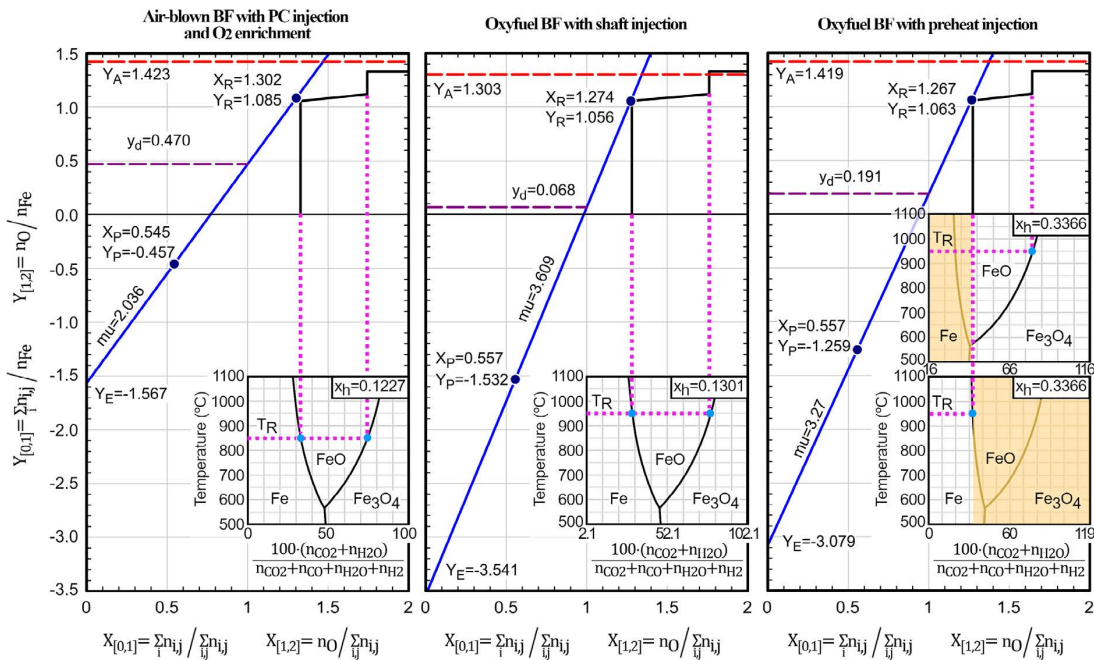
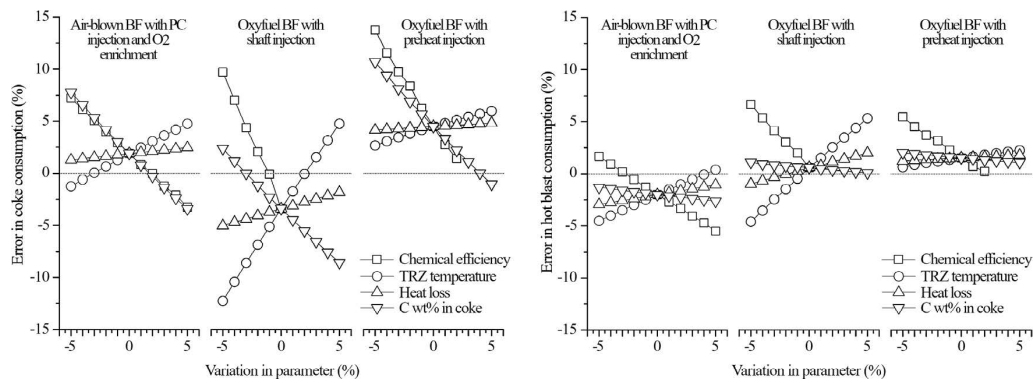


Fig. 5. Extended operating lines obtained for an air-blown BF with PC injection,<sup>28)</sup> an oxyfuel BF with shaft injection,<sup>14)</sup> and an oxyfuel BF with preheat injection.<sup>16)</sup> (Online version in color.)

Table 5. Comparison of the data derived from the operating line for the original Rist diagram and for the new extended operating diagram.

	BF with PC injection			OBF with Shaft injection			OBF with Preheat injection		
	Babich <sup>28)</sup>	Rist diagram	Extended diagram	Jin <sup>14)</sup>	Rist diagram	Extended diagram	Sato <sup>16)</sup>	Rist diagram	Extended diagram
Coke (kg/thm)	283.0	288.3	288.3	183.0	219.1	176.7	232.0	275.2	242.4
Hot blast (kg/thm)	1 172.1	1 148.6	1 148.6	312.1	350.4	313.9	420.6	363.1	427.0
Direct reduction (%)	–	33.0	33.0	–	0.8	5.2	–	3.6	13.5
Gas utilization (%)	48.6	46.8	46.8	38.4	34.0	37.4	–	40.0	53.6



**Fig. 6.** Error in the calculated values of coke and hot blast consumptions, as a function of percentage variations on different parameters, for an air-blown BF with PC injection,<sup>28)</sup> an oxyfuel BF with shaft injection,<sup>14)</sup> and an oxyfuel BF with preheat injection.<sup>16)</sup>

no mid or upper injections), and because (ii) there are no oxidized gases at the beginning of the indirect reduction process (*i.e.*, no  $\text{CO}_2$  or  $\text{H}_2\text{O}$  right after the raceways). These two conditions are the hypothesis assumed during the construction of the original Rist diagram, therefore it provides good results in this case. Indeed, this data set was selected to show that the extended model correctly reproduces the particular case described by the hypotheses of the original Rist model.

In the second data set (OBF with shaft injection), the error obtained by the original Rist model is between 10% and 20%, while the extended model gives an error below 3.4%. The original Rist model assumes that all the  $\text{CO}_2$  and  $\text{H}_2\text{O}$  injected will be dissociated to  $\text{CO}$  and  $\text{H}_2$  by consuming  $\text{C}$ . However, it is actually not the case for the injection taking place in the shaft zone. Moreover, since the dissociation is endothermic, the original Rist model additionally increases the coke consumption to keep the energy balance. For these reasons, the necessary coke predicted by the original Rist diagram is overestimated, as well as the required oxygen (used to burnt the coke that provides the energy for the dissociation).

In the third data set (OBF with preheat injection), the error obtained through the original Rist model is between 14% and 19%, while the extended model gives an error below 4.5%. As in the previous case, the presence of  $\text{CO}_2$  and  $\text{H}_2\text{O}$  in the injection is the reason of overestimating the necessary coke. In practice, this  $\text{CO}_2$  is not present in the raceways (*i.e.*, will not ascend in the form of  $\text{CO}$  acting as a reducing gas), so we still need to burn coke with oxygen to produce the necessary  $\text{CO}$ . Thus, the  $\text{O}_2$  flow is greater in the actual data (and in the extended model) than in the original Rist diagram, since the latter assumes that part of the  $\text{O}_2$  comes from the  $\text{CO}_2$  (Eq. (13)) when in practice is actually not.

In both OBF data sets, the percentage of direct reduction predicted by the original Rist diagram is underestimated, as it was explained at the end of section 2.1. Similarly, the gas utilization obtained by the original Rist diagram is lower than the actual value because the operating line in the range  $1 < X < 2$  only takes into account the  $\text{CO}_2$  and  $\text{H}_2\text{O}$  coming from the reduction of iron ore, and not from the injections. Thus, the higher the amount of  $\text{CO}_2$  and  $\text{H}_2\text{O}$  in the injections, the higher these two errors.

### 5.3. Influence of the Input Data Uncertainty on the Results of the Extended Operating Diagram

The discrepancy between the reference data and the results of the extended operating diagram might be reduced with more detailed data sets (composition of inlet streams, chemical efficiency, temperature of the thermal reserve zone, and heat loss profile). The assumed data may play an important role when decreasing the error between the real data and the model results. The Fig. 6 shows the influence

of different parameters on the calculated values of coke and hot blast consumption.

Regarding the calculation of coke consumption, the most significant parameters are the chemical efficiency and the composition of the coke ( $\text{C}$  wt% content). Uncertainty of 1% in these inputs may vary the final error by 1.1–2.6 percentage points. The temperature of the thermal reserve zone has also a remarkable influence (especially in the case of shaft injections), since 1% uncertainty may increase the error in the coke consumption by up to 1.7 percentage points.

Regarding the calculation of the hot blast consumption, the influence of the input parameters is much lower. In this case, only the uncertainty of the chemical efficiency and the TRZ temperature are relevant when aiming for reducing the final error of the model. An uncertainty of 1% in the chemical efficiency lead to changes of 0.7–1.2 percentage points in the error of the hot blast consumption. If the uncertainty is in the TRZ temperature, the error of the calculated value may vary by 0.2–1.0 percentage points, per 1% of uncertainty in the input data.

## 6. Conclusions

In this article we proposed a generalization of the operating line methodology to extend its applicability to scenarios of variable molar flows along the blast furnace (*i.e.*, shaft and preheating injections) and non-continuous oxidation profiles (presence of  $\text{CO}_2$  and  $\text{H}_2\text{O}$  in the injected gases). To do so, we redefined the operating diagram by considering the mole flow of the final blast furnace gas in the region  $0 < X < 1$  (instead of only the mole flow of  $\text{CO}$  and  $\text{H}_2$  after the raceways), and the transfer of  $\text{O}$  atoms from the iron ore to the gas in the region  $1 < X < 2$  (rather than the oxidation state of the gas). This way, we combined the two regions of the Cartesian diagram by using the quotient between the mole flow of the final blast furnace gas and the moles of  $\text{Fe}$  produced in the blast furnace, which remains constant independently of the place, type and number of gas injections.

The extended operating line methodology was implemented in an Aspen Plus simulation, which provides a detailed modelling of the preparation zone, the thermal reserve zone, the lower zone and the raceways. The simulation was used to validate the generalized diagram through three different data sets: (i) an air-blown blast furnace with pulverized coal injection and  $\text{O}_2$  enrichment, (ii) an oxyfuel blast furnace with gas injection in the thermal reserve zone, and (iii) an oxyfuel blast furnace with gas injection in the preparation zone. The former was included to show that the generalized methodology can also replicates the results of the conventional operating diagram.

In general, the error between the reference data and the simulation results is well below 3.5%, so the extended operating line methodology has been validated. In addi-

tion, the proposed Aspen plus model has proven to be a valid approach for the simulation of blast furnaces, since it correctly quantifies the inlet and outlet streams of the preparation zone, the thermal reserve zone, the lower zone and the raceways. As a recommendation, the uncertainty in the input data of the model should be kept as low as possible (chemical efficiency, TRZ temperature, and coke composition), since variations of 1% in these values may lead to increments of 0.2–2.6 percentage points in the final error of the model.

### Acknowledgements

This project has received funding from the European Union's Framework Programme for Research and Innovation Horizon 2020 (2014–2020) under the Marie Skłodowska-Curie Grant Agreement No. 887077.

### Nomenclature

In this paper we used calorie as unit of energy for calculations related to operating diagram in order to facilitate comparing results with the original work of Rist. Elsewhere, SI units are used.

#### Acronyms

BF: blast furnace (air-blown, unless otherwise specified)

BFG: blast furnace gas

HB: hot blast

HM: hot metal

NIST: National Institute of Standards and Technology

OBF: oxyfuel blast furnace

PC: pulverized coal

THM: ton of hot metal

TRZ: thermal reserve zone

#### Symbols

A: calculation parameter, kcal/mol

$a_j$ : number of moles of H<sub>2</sub> in injectant  $j$  per number of moles of injectant  $j$ , mol<sub>H<sub>2</sub></sub>/mol <sub>$j$</sub>

B: calculation parameter, kcal/mol

$b_j$ : number of moles of O<sub>2</sub> in injectant  $j$  per number of moles of injectant  $j$ , mol<sub>O<sub>2</sub></sub>/mol <sub>$j$</sub>

C: calculation parameter, kcal/mol

$C_{\Delta T_R}$ : sensible heat of the burden between  $T_R - \Delta T_R$  and  $T_R$  (lack of thermal ideality), kcal/mol<sub>Fe</sub>

D: calculation parameter, –

$e$ : number of moles of H<sub>2</sub>O per number of atoms of O in the air (i.e.,  $e = y_e/y_v$ ), mol<sub>H<sub>2</sub>O</sub>/mol<sub>O</sub>

E: calculation parameter, –

$f$ : sensible heat of the hot metal between  $T_R$  and  $T_f$  (outlet temperature), kcal/mol<sub>Fe</sub>

F: calculation parameter, –

$l$ : sensible heat of the slag between  $T_R$  and  $T_l$  (outlet temperature), kcal/mol<sub>Fe</sub>

$m$ : mass flow, kg/t<sub>HM</sub>

$M$ : molar weight, kg/kmol

$n_{Fe}$ : number of moles of Fe produced in the blast furnace per ton of hot metal, mol<sub>Fe</sub>/t<sub>HM</sub>

$n_{i,j}$ : number of moles of component  $i$  produced by the reaction or injection  $j$  per ton of hot metal, mol/t<sub>HM</sub>

$n_O$ : number of atoms of O transferred from the burden to the gas per ton of hot metal, mol<sub>O</sub>/t<sub>HM</sub>

$p$ : heat removed by the staves in the elaboration zone, kcal/mol<sub>Fe</sub>

$q_c$ : heat released at  $T_R$  by the reaction C (coke) + 0.5 O<sub>2</sub> → CO, kcal/mol<sub>O</sub>

$q_e$ : heat required by the H<sub>2</sub>O in hot blast due to dissociation, reverse water-gas shift and sensible heat, kcal/mol<sub>H<sub>2</sub>O</sub>

$q_g$ : heat absorbed at  $T_R$  by the reaction C + CO<sub>2</sub> → 2CO, kcal/mol<sub>C</sub>

$q_{iw}$ : heat released at  $T_R$  by the reaction Fe<sub>0.95</sub>O + CO → 0.95 Fe + CO<sub>2</sub>, kcal/mol<sub>O</sub>

$q_j$ : thermal demand by injectant  $j$ , CH<sub>2a</sub>O<sub>2b</sub>N<sub>2c</sub>S<sub>2d</sub>Z<sub>z</sub>

(or H<sub>2a</sub>O<sub>2b</sub>N<sub>2c</sub> or O<sub>2b</sub>N<sub>2c</sub>) due to dissociation, sensible heat, reverse water-gas shift of the H<sub>2</sub>, incomplete combustion with the O<sub>2</sub>, and transfer of S to the slag, kcal/mol <sub>$j$</sub>

$q_j$ : heat absorbed at  $T_R$  by the total H<sub>2</sub> in the furnace when considering that it is completely converted to H<sub>2</sub>O through the reverse water-gas shift reaction, kcal/mol<sub>H<sub>2</sub></sub>

$q_{mid}$ : energy consumption to heat the shaft injection to  $T_R$ , kcal/mol<sub>mid</sub>

$q_{Mn}$ : heat absorbed at  $T_R$  by the reaction C + MnO → CO + Mn, kcal/mol<sub>O</sub>

$q_p$ : heat absorbed at  $T_R$  by the reaction 1/5P<sub>2</sub>O<sub>5</sub>·3CaO + C + 6/5Fe → 2/5Fe<sub>3</sub>P + 3/5CaO + CO, kcal/mol<sub>O</sub>

$q_{Si}$ : heat absorbed at  $T_R$  by the reaction C + 1/2SiO<sub>2</sub> + 3/2Fe → CO + 1/2Fe<sub>3</sub>Si, kcal/mol<sub>O</sub>

$q_s$ : energy available from the sensible heat of the air between  $T_v$  and  $T_R$ , kcal/mol<sub>O</sub>

$q_{\gamma}$ : heat absorbed at  $T_R$  by the carburization of the iron, kcal/mol<sub>C</sub>

$r$ : chemical efficiency of the blast furnace, –

$T_R$ : temperature of the thermal reserve zone, °C

$\Delta T_R$ : difference of temperature between the gas and the solid at the beginning of the middle zone, °C

$T_v$ : temperature of the hot blast, °C

$X$ : abscissa in the extended operating diagram, –

$x_{CO_2,j}$ : number of moles of CO<sub>2</sub> entering with injectant  $j$ , per mole of BFG (excl. N<sub>2</sub>), mol<sub>CO<sub>2</sub></sub>/mol<sub>BFG</sub>

$x_d$ : number of moles of CO produced via direct reduction, per mole of BFG (excl. N<sub>2</sub>), mol<sub>CO</sub>/mol<sub>BFG</sub>

$x_e$ : number of moles of H<sub>2</sub>O in hot blast, per mole of BFG (excl. N<sub>2</sub>), mol<sub>H<sub>2</sub>O</sub>/mol<sub>BFG</sub>

$x_h$ : molar fraction of hydrogen and water in gas mixture at the thermal reserve zone, –

$x_{H_2O,j}$ : number of moles of H<sub>2</sub>O entering with injectant  $j$ , per mole of BFG (excl. N<sub>2</sub>), mol<sub>H<sub>2</sub>O</sub>/mol<sub>BFG</sub>

$x_i$ : number of moles of O atoms removed from burden by indirect reduction, per mole of BFG (excl. N<sub>2</sub>), mol<sub>O</sub>/mol<sub>BFG</sub>

$x_j$ : number of moles of injectant  $j$ , per mole of BFG (excl. N<sub>2</sub>), mol <sub>$j$</sub> /mol<sub>BFG</sub>

$x_k$ : number of moles of H<sub>2</sub> in the coke, per mole of BFG (excl. N<sub>2</sub>), mol<sub>H<sub>2</sub></sub>/mol<sub>BFG</sub>

$x_{mb}$ : number of moles of moisture in the burden, per mole of BFG (excl. N<sub>2</sub>), mol<sub>H<sub>2</sub>O</sub>/mol<sub>BFG</sub>

$x_{mid}$ : number of moles of injection in the mid zone, per mole of BFG (excl. N<sub>2</sub>), mol<sub>MID</sub>/mol<sub>BFG</sub>

$x_{Mn}$ : number of moles of CO produced via the direct reduction of MnO, per mole of BFG (excl. N<sub>2</sub>), mol<sub>CO</sub>/mol<sub>BFG</sub>

$x_p$ : number of moles of CO produced via the direct reduction of P<sub>2</sub>O<sub>5</sub>, per mole of BFG (excl. N<sub>2</sub>), mol<sub>CO</sub>/mol<sub>BFG</sub>

$x_s$ : number of moles of CO produced via the transfer of S to the slag, per mole of BFG (excl. N<sub>2</sub>), mol<sub>CO</sub>/mol<sub>BFG</sub>

$x_{Si}$ : number of moles of CO produced via the direct reduction of SiO<sub>2</sub>, per mole of BFG (excl. N<sub>2</sub>), mol<sub>CO</sub>/mol<sub>BFG</sub>

$x_{up}$ : number of moles of injection in the preparation zone, per mole of BFG (excl. N<sub>2</sub>), mol<sub>UP</sub>/mol<sub>BFG</sub>

$x_v$ : number of moles of CO produced by the O<sub>2</sub> of the hot blast via the combustion of C, per mole of BFG (excl. N<sub>2</sub>), mol<sub>CO</sub>/mol<sub>BFG</sub>

Y: ordinate in the extended operating diagram, –

$Y_A$ : initial oxidation state of the burden, mol<sub>O</sub>/mol<sub>Fe</sub>

$y_{CO_2,j}$ : number of moles of CO<sub>2</sub> entering with injectant  $j$ , per mole of Fe produced, mol<sub>CO<sub>2</sub></sub>/mol<sub>Fe</sub>

$y_{CO_2,mid}$ : number of moles of CO<sub>2</sub> entering with gas injected at mid zone, per mole of Fe produced, mol<sub>CO<sub>2</sub></sub>/mol<sub>Fe</sub>

$y_{CO_2,up}$ : number of moles of CO<sub>2</sub> entering with gas injected at upper zone, per mole of Fe produced, mol<sub>CO<sub>2</sub></sub>/mol<sub>Fe</sub>

$y_d$ : number of moles of CO produced via direct reduction, per mole of Fe produced, mol<sub>CO</sub>/mol<sub>Fe</sub>

$y_{d,\%}$ : percentage of O atoms removed from iron oxides by direct reduction, %

$y_e$ : number of moles of H<sub>2</sub>O in hot blast, per mole of Fe produced, mol<sub>H<sub>2</sub>O</sub>/mol<sub>Fe</sub>

$Y_E$ : intercept of the extended operating line, –

$Y_E^*$ : terms of  $Y_E$  that are independent of  $y_v$ , –

$y_{H_2O,j}$ : number of moles of H<sub>2</sub>O entering with injectant  $j$ , per mole of Fe produced, mol<sub>H<sub>2</sub>O</sub>/mol<sub>Fe</sub>

$y_{H_2O,mid}$ : number of moles of H<sub>2</sub>O entering with gas injected at mid zone, per mole of Fe produced, mol<sub>H<sub>2</sub>O</sub>/mol<sub>Fe</sub>

$y_{H_2O,up}$ : number of moles of H<sub>2</sub>O entering with gas injected at upper zone, per mole of Fe produced, mol<sub>H<sub>2</sub>O</sub>/mol<sub>Fe</sub>

$y_i$ : number of moles of O atoms removed from burden by indirect reduction, per mole of Fe produced, mol<sub>O</sub>/mol<sub>Fe</sub>

$y_j$ : number of moles of injectant  $j$ , per mole of Fe produced, mol<sub>j</sub>/mol<sub>Fe</sub>

$y_k$ : number of moles of H<sub>2</sub> in the coke, per mole of Fe produced, mol<sub>H<sub>2</sub></sub>/mol<sub>Fe</sub>

$y_{mb}$ : number of moles of moisture in the burden, per mole of Fe produced, mol<sub>H<sub>2</sub>O</sub>/mol<sub>Fe</sub>

$y_{mid}$ : number of moles of injection in the mid zone, per mole of Fe produced, mol<sub>MID</sub>/mol<sub>Fe</sub>

$y_{Mn}$ : number of moles of CO produced via the direct reduction of MnO, per mole of Fe produced, mol<sub>CO</sub>/mol<sub>Fe</sub>

$y_P$ : number of moles of CO produced via the direct reduction of P<sub>2</sub>O<sub>5</sub>, per mole of Fe produced, mol<sub>CO</sub>/mol<sub>Fe</sub>

$y_S$ : number of moles of CO produced via the transfer of S to the slag, per mole of Fe produced, mol<sub>CO</sub>/mol<sub>Fe</sub>

$y_{Si}$ : number of moles of CO produced via the direct reduction of SiO<sub>2</sub>, per mole of Fe produced, mol<sub>CO</sub>/mol<sub>Fe</sub>

$y_{up}$ : number of moles of injection in the preparation zone, per mole of Fe produced, mol<sub>UP</sub>/mol<sub>Fe</sub>

$y_v$ : number of moles of CO produced by the O<sub>2</sub> of the hot blast via the combustion of C, per mole of Fe produced, mol<sub>CO</sub>/mol<sub>Fe</sub>

Greek symbols

$\gamma$ : number of moles of C dissolved in the hot metal, mol<sub>C</sub>/mol<sub>Fe</sub>

$\delta$ : decrease in the available heat due to the presence of magnetite in the elaboration zone, kcal/mol<sub>Fe</sub>

$\delta'$ : decrease in the heat absorbed by the reverse water-gas shift reaction because of the lack of chemical ideality, kcal/mol<sub>Fe</sub>

$\mu$ : slope of the extended operating diagram (moles of BFG, excl. N<sub>2</sub>, per mol of Fe produced), mol<sub>BFG</sub>/mol<sub>Fe</sub>

$\eta_{CO,H_2}$ : gas utilization factor, –

$\tau_j$ : calculation parameter that is 1 when the auxiliary injection  $j$  contains carbon and 0 when not, –

$\omega$ : molar fraction or oxidation state, –

$\Omega_{j,i}$ : mass fraction of compound  $i$  in stream  $j$ , –

Subscripts and superscripts

K: coke

OC: related to the equilibrium of CO and CO<sub>2</sub> with pure wüstite

OH: related to the equilibrium of H<sub>2</sub> and H<sub>2</sub>O with pure wüstite


OHC: related to the equilibrium of CO, CO<sub>2</sub>, H<sub>2</sub> and H<sub>2</sub>O with pure wüstite


P: characteristic point of the extended operating line related to the energy balance of the elaboration zone

R: characteristic point of the extended operating line related to the thermal reserve zone

W: referring to the chemical reserve zone (pure wüstite is in equilibrium with the gas)

ORCID

Manuel BAILERA  <https://orcid.org/0000-0002-9174-9820>

Takao NAKAGAKI  <https://orcid.org/0000-0001-8008-7238>

REFERENCES

- 1) International Energy Agency: Iron and Steel Technology Roadmap, IEA, Paris, (2020), 1.
- 2) M. A. Quader, S. Ahmed, R. A. R. Ghazilla, S. Ahmed and M. Dahari: *Renew. Sustain. Energy Rev.*, **50** (2015), 594. <https://doi.org/10.1016/j.rser.2015.05.026>
- 3) K. De Ras, R. Van de Vijver, V. V. Galvita, G. B. Marin and K. M. Van Geem: *Curr. Opin. Chem. Eng.*, **26** (2019), 81. <https://doi.org/10.1016/j.coche.2019.09.001>
- 4) M. D. Fenton and C. A. Tuck: 2016 Minerals Yearbook, US Geological Survey, Reston, (2019), 37.1.
- 5) Q. Wang, Y. Zhu, Q. Wu, E. Gratz and Y. Wang: *RSC Adv.*, **5** (2015), 5501. <https://doi.org/10.1039/C4RA14576C>
- 6) A. Babich, D. Senk, H. Gudenau and K. T. Mavrommatis: Ironmaking Textbook, RWTH Aachen University, Aachen, (2008), 1.
- 7) M. Geerdes, R. Chaigneau, O. Lingardi, R. Molenaar, R. van Opbergen, Y. Sha and P. Warren: Modern Blast Furnace Ironmaking, An Introduction, IOS Press, Amsterdam, (2020), 1.
- 8) F. Ueckerdt, C. Bauer, A. Dirnaichner, J. Everall, R. Sacchi and G. Luderer: *Nat. Clim. Chang.*, **11** (2021), 384. <https://doi.org/10.1038/s41558-021-01032-7>
- 9) S. Hisashige, T. Nakagaki and T. Yamamoto: *ISIJ Int.*, **59** (2019), 598. <https://doi.org/10.2355/isijinternational.ISIJINT-2018-355>
- 10) D. C. Rosenfeld, H. Böhm, J. Lindorfer and M. Lehner: *Renew. Energy*, **147** (2020), 1511. <https://doi.org/10.1016/j.renene.2019.09.053>
- 11) M. Bailera, P. Lisbona, B. Peña and L. M. Romeo: *J. CO<sub>2</sub> Util.*, **46** (2021), 101456. <https://doi.org/10.1016/j.jcou.2021.101456>
- 12) J. Perpiñán, M. Bailera, L. M. Romeo, B. Peña and V. Evely: *Energies*, **14** (2021), 7090. <https://doi.org/10.3390/en14217090>
- 13) M. Helle and H. Saxén: *ISIJ Int.*, **55** (2015), 2047. <https://doi.org/10.2355/isijinternational.ISIJINT-2015-083>
- 14) P. Jin, Z. Jiang, C. Bao, Y. Lu, J. Zhang and X. Zhang: *Steel Res. Int.*, **87** (2016), 320. <https://doi.org/10.1002/srin.201500054>
- 15) H. Wang, M. Chu, T. Guo, W. Zhao, C. Feng, Z. Liu and J. Tang: *Steel Res. Int.*, **87** (2016), 539. <https://doi.org/10.1002/srin.201500372>
- 16) M. Sato, K. Takahashi, T. Nouchi and T. Ariyama: *ISIJ Int.*, **55** (2015), 2105. <https://doi.org/10.2355/isijinternational.ISIJINT-2015-264>
- 17) T. Ariyama, M. Sato, T. Nouchi and K. Takahashi: *ISIJ Int.*, **56** (2016), 1681. <https://doi.org/10.2355/isijinternational.ISIJINT-2016-210>
- 18) A. Rist and N. Meysson: *J. Met.*, **19** (1967), 50. <https://doi.org/10.1007/bf03378564>
- 19) M. Bailera, T. Nakagaki and R. Kataoka: *Open Res. Eur.*, **1** (2021), 141. <https://doi.org/10.12688/openreseurope.14275.1>
- 20) H. Zhang, H. Li, Q. Tang and W. Bao: *Sci. China Technol. Sci.*, **53** (2010), 85. <https://doi.org/10.1007/s11431-010-0029-0>
- 21) K. Suzuki, K. Hayashi, K. Kuribara, T. Nakagaki and S. Kasahara: *ISIJ Int.*, **55** (2015), 340. <https://doi.org/10.2355/isijinternational.55.340>
- 22) C. Yilmaz, J. Wendelstorf and T. Turek: *J. Clean. Prod.*, **154** (2017), 488. <https://doi.org/10.1016/j.jclepro.2017.03.162>
- 23) N. Müller, G. Herz, E. Reichelt and M. Jahn: DGMM Tagungsbericht (Proc. DGMM Conf.), DGMM, Hamburg, (2018), 187.
- 24) M. Bailera, T. Nakagaki and R. Kataoka: Zenodo, CERN, (2021), <https://doi.org/10.5281/zenodo.5637580>
- 25) Aspen Technology, Inc.: Aspen Physical Property Methods - Reference Manual, AspenTech, Bedford, MA, (2019), 1.
- 26) Aspen Technology, Inc.: Physical Property Models - Reference Manual, AspenTech, Bedford, MA, (2019), 1.
- 27) D. W. Green and M. Z. Southard: Perry's Chemical Engineers' Handbook, 9th ed., McGraw-Hill Education, New York, (2019), 1.
- 28) A. Babich, D. Senk, J. Solar and I. de Marco: *ISIJ Int.*, **59** (2019), 2212. <https://doi.org/10.2355/isijinternational.ISIJINT-2019-337>
- 29) S. Kasahara, Y. Inagaki and M. Ogawa: *ISIJ Int.*, **52** (2012), 1409. <https://doi.org/10.2355/isijinternational.52.1409>